Lithos 318–319 (2018) 91–103

Contents lists available at ScienceDirect

Lithos

journal homepage: www.elsevier.com/locate/lithos

Magnesium isotopic composition of continental arc andesites and the implications: A case study from the El Laco volcanic complex, Chile

Qiuhong Xie [a], Zhaochong Zhang [a,*], Eduardo Campos [b], Zhiguo Cheng [a], Xianghui Fei [a], Bingxiang Liu [a], Yiran Qiu [c], M. Santosh [a,d], Shan Ke [a], Lijuan Xu [a]

[a] State Key Laboratory of Geological Processes and Mineral Resources, China University of Geosciences, Beijing 100083, China
[b] Departamento de Ciencias Geológicas, Universidad Católica del Norte, Antofagasta 1240000, Chile
[c] Shandong 5th Geo-Mineral Prospecting Institute, Tai'an 271000, China
[d] Department of Earth Sciences, University of Adelaide, Adelaide, SA 5005, Australia

ARTICLE INFO

Article history:
Received 15 February 2018
Accepted 6 August 2018
Available online 10 August 2018

Keywords:
Continental arc andesites
Magnesium isotopes
Altered oceanic basalt
El Laco volcanic complex

ABSTRACT

Continental crust can dramatically modify the geochemical and isotopic compositions (e.g., Sr-Nd, Pb) of mantle-derived lavas, and has important implications in understanding magmatic processes in continental arcs which involve subducted materials. In this paper, we report the Mg isotopic compositions of continental arc andesites from El Laco in northern Chile, and evaluate the contribution of the subducted slab to the formation of continental arc lavas. The andesites in the El Laco volcanic complex (ELVC) display relatively high $(^{87}Sr/^{86}Sr)_i$ ratios and negative age-corrected $\varepsilon_{Nd}(t)$ ($t = 1.6$ Ma) values. The $\delta^{26}Mg$ values of the ELVC andesites range from $-0.26 \pm 0.05‰$ to $-0.15 \pm 0.04‰$ (average $\delta^{26}Mg = -0.18 \pm 0.05‰$), slightly heavier than that of the primitive mantle. The $\delta^{26}Mg$ values of clinopyroxene, orthopyroxene and magnetite grains separated from andesites are $-0.27 \pm 0.03‰$ to $-0.20 \pm 0.04‰$, $-0.24 \pm 0.06‰$ to $-0.18 \pm 0.03‰$ and $+0.09 \pm 0.06‰$ to $+0.33 \pm 0.06‰$, respectively. Our results suggest that Mg isotope fractionation occurred during the fractional crystallization of El Laco andesite, and imply complex Mg isotopic fractionation at high-temperature conditions than previously inferred. Combing the Mg isotopes with the geochemical and Sr-Nd isotopic data, we confirm that neither the deep process of partial melting nor the shallow process of crust contamination contributed to the heavier Mg isotopes of the andesites. The heavier Mg isotopic features of these lavas were mainly inherited from aqueous fluids derived from the subducted slab, which reacted with the primitive mantle wedge to produce a metasomatic mantle source for the continental arc lavas.

1. Introduction

Continental arc volcanism contributes significantly to the crustal accretion, and an archive of the elemental cycling between the subducting slab and the subarc mantle (e.g., Wei et al., 2017). Andesites are the major components of continental volcanic arcs (Rudnick, 1995; Zhu et al., 2013), and although they have been extensively studied, the role of the subducted slab in the petrogenesis of the continental arc andesites remains a subject of debate. The diverse models proposed for the origin of these andesites can be generally grouped into two. One is the basalt input model, which postulates that geological processes including magma mixing, e.g., a mixture of basaltic melt and crust-derived silicic melt (Reubi and Blundy, 2009), and/or the assimilation fractional crystallization (AFC) processes of a mantle-derived melt (e.g., Hildreth and Moorbath, 1988; Lee et al., 2007) are necessary to produce such andesites. The other is a primitive andesite model, which suggests that the subducted oceanic crust plays a critical role in the formation of new crust and the arc andesitic lavas (e.g., Grove et al., 2002, 2012; Kelemen, 1995; Kelemen et al., 2003; Tatsumi, 2006; Taylor, 1967). Both models invoke the incorporation of crustal materials, containing continental crust and/or oceanic crust, in the petrogenesis of the arc andesites. Considering the relatively thick continental crust in orogenic belts, incorporation of the continental crust into the mantle-derived magmatic system is generally significant. Since many incompatible elements including Nd, Sr and Pb are substantially more enriched in the crust than in mantle peridotite, the geochemical and Sr-Nd-Pb isotopic compositions of arc lavas derived from the mantle tend to be significantly modified by crustal contamination and/or magma mixing of crust-derived silicic melts.

Magnesium is one of the major elements found in the crust and in the mantle, having three isotopes: ^{24}Mg, ^{25}Mg and ^{26}Mg. Previous studies have shown limited Mg isotope fractionation during high-temperature igneous process (Handler et al., 2009; Teng et al., 2007, 2010a; Wang et al., 2014; Yang et al., 2009), with different reservoirs exhibiting distinct Mg isotopic compositions (Teng, 2017). Thus, the Mg isotopes are recognized as a powerful proxy to trace the sources,

* Corresponding author.
E-mail address: zczhang@cugb.edu.cn (Z. Zhang).

https://doi.org/10.1016/j.lithos.2018.08.010
0024-4937/

and have the potential to provide important constrains on the processes operating during the formation of continental arc andesites.

Andesites are among the typical continental arc magma in the world such as those in the Andes cordillera, located along the western margin of the South American plate. The Pliocene-Early Pleistocene andesitic lavas of ELVC, in northern Chile, are part of the Central Volcanic Zone (CVZ) of the Andes (Fig. 1; Tornos et al., 2016; Velasco et al., 2016), and provide good example to constrain the deep processes of arc andesites. Here, for the first time, we report the Mg isotopic compositions of continental arc andesites in the Andes. Combining Mg isotopes and geochemical and Sr-Nd isotopic data, we demonstrate that both the continental and oceanic crust contributed substantially to the formation of the continental arc lavas.

2. Geological setting and petrography

The formation of the Andes Cordillera resulted from the eastward subduction of an oceanic plate (i.e., the Nazca plate in Fig. 1) beneath

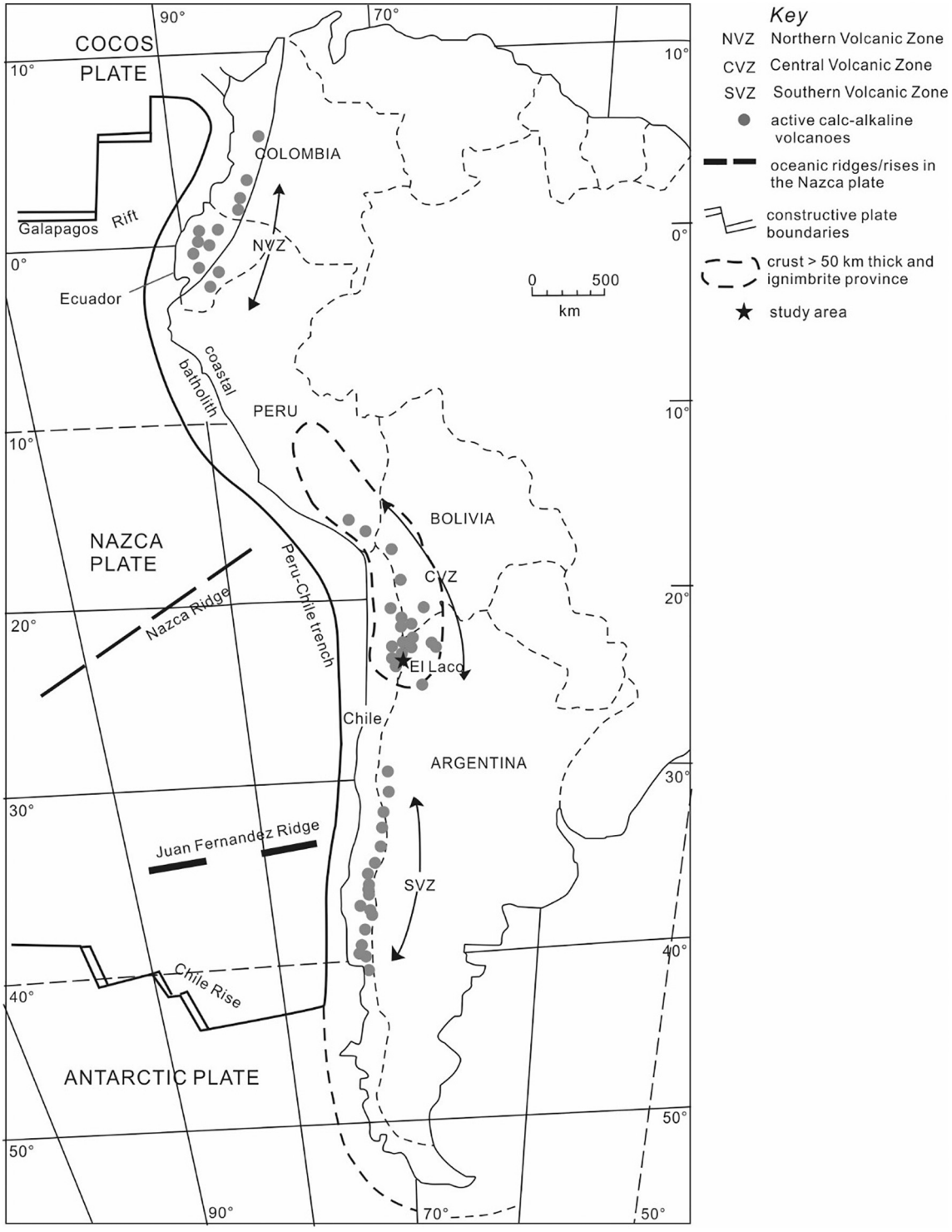

Fig. 1. Distribution of active volcano zones along the Andean Cordillera. (Modified from Wilson (1989).)

the western margin of South America since the Mesozoic. The Andes extends for about 7000 km along the western margin of the continent, making it the longest sub-aerial mountain chain on Earth. As shown in Fig. 1, volcanism of the Andes has been divided into the Northern Volcanic Zone (NVZ) from 5°N to 2°S, the Central Volcanic Zone (CVZ) extending from 16°S to 28°S in southern Peru, northern Chile, Bolivia and Argentina, and the Southern Volcanic Zone (SVZ) in southern Chile and Argentina. In each zone, volcanism has occurred episodically since the Mesozoic. The NVZ lavas are dominantly basaltic andesites and andesites. In general, the most common rock types of the SVZ are similar but slightly more basic, mainly composed of high-alumina basalt and basaltic andesite. The CVZ lavas are characteristically intermediate to felsic in composition and calc-alkaline, showing a marked increase in K_2O content (at constant SiO_2 content) with an increasing depth to the Benioff zone (e.g., Wilson, 1989).

The ELVC in the CVZ in northern Chile (lat. 23°48′S, long. 67°30′W, Fig. 2), is located within the current N-S-trending High Andes volcanic arc. This arc has been active since the Late Oligocene and was the product of the subduction of the Nazca Plate in the Late Cenozoic, when the tectonic and magmatic effects of the Andean tectonism migrating eastward reached this area (Frutos and Oyarzún, 1975). A key feature of the CVZ is the presence of an exceptionally (up to 70–80 km) thick continental crust (Zandt et al., 1994), which was the product of the middle Miocene tectonic thickening (Allmendinger et al., 1997; Trumbull et al., 1999). The crustal thickness beneath the ELVC is ~60 km (Tassara, 1997), and the depth to the well-defined Benioff zone beneath the volcano is approximately 125 km (Frutos et al., 1990). The basement beneath the ELVC consists mainly of Lower Ordovician to Upper Silurian sedimentary formations of marine platform facies, including principally fossiliferous quartzite and mica-rich sandstone with some sedimentary iron strata. Strata overlying unconformably on the Paleozoic series are the Mesozoic and Cenozoic detrital continental sediments and the extensive Upper Tertiary rhyolitic flows (Frutos and Oyarzún, 1975). Small evaporitic basins are common in high Altiplano area around El Laco. Moreover, glacial deposits are present to the west of the El Laco, and glacial erosion has removed the upper part of the volcano.

The ELVC consists of a stratovolcanic deposition of andesites followed by the slow extrusion of a rhyodacitic central needle (Fig. 2b). It is located at an elevation between 4600 and 5472 m, covering an area of over 35 km^2 with a volume of at least 14 km^3. The ELVC andesites formed during the Pliocene-Early Pleistocene and show whole rock K-Ar ages ranging from 5.3 ± 1.9 Ma to 1.6 ± 0.5 Ma (Naranjo et al., 2010). The andesitic rocks are gray to black in hand specimen (Fig. 3a), and exhibit porphyritic texture and vesicular structure. The phenocrysts (30–40 vol%) are dominantly composed of plagioclase (50–60 vol%, some with normal or oscillatory zoning), clinopyroxene (25–30 vol%) and orthopyroxene (15–20 vol%) (Fig. 3b–e). The groundmass displays a hyalopilitic texture, consisting of glass, magnetite, rare apatite and microcrystals of plagioclase, orthopyroxene and clinopyroxene. Ilmenite lamellae occur in magnetite, and some magnetite and rare apatite grains occasionally occur as inclusions enclosed by the phenocrysts (Fig. 3f).

3. Sampling and analytical methods

Eight samples of unaltered andesite were collected around the Pico Laco at the altitude of 5005 m whereas the LcSur-3 sample was collected near the Laco Sur iron deposit at an altitude of 4698 m (Fig. 2a). The rocks were pulverized for bulk major and trace elements, as well as Sr-Nd and Mg isotopes, whereas magnetite and phenocrysts of clinopyroxene and orthopyroxene were separated from the fresh andesite for analyzing the Mg isotopes.

3.1. Mineral chemistry

Electron microprobe analyses of plagioclase, clinopyroxene, orthopyroxene and the co-growing mineral pairs of magnetite and ilmenite were conducted using the JXA-8230 electron microprobe with the wavelength dispersive (WDS) technique at the Chinese Academy of Geological Sciences. The operating conditions were set as follow: 15 kV accelerating voltage, 10 nA beam current, 1–5 μm beam diameter and 5 s counting times on backgrounds. Elements were standardized on natural minerals or the synthetic oxides national standards. The measured data were corrected using the ZAF correction procedure after Armstrong (1995) and the precision is better than 1 wt% for element oxide.

3.2. Major and trace elements

The rocks selected for bulk-rock analysis were crushed and ground to ~200 mesh. Bulk-rock major and trace elemental analyses were determined at the National Research Centre for Geoanalysis, Beijing. Major element analysis was obtained by X-ray fluorescence spectrometer (XRF) using the PW4400 where the analytical uncertainties ranged from 1% to 3%. Loss on ignition (LOI) was determined gravimetrically after the samples were heated at 980 °C for 30 min. The detailed procedure of the major elemental analyses was as reported by Norrish and Chappell (1977). Trace elements were analyzed by using the PE300D inductively coupled plasma mass spectrometry (ICP-MS) with an X-series instrument, with the similar analytical procedure as described by Qi et al. (2000). The precision is generally better than 5% RSD (relative standard deviation) for most elements.

3.3. Isotopic compositions

Strontium and Nd isotopic compositions of whole rocks were carried out on MC-ICP-MS at the State Key Laboratory of Geological Processes and Mineral Resources, China University of Geosciences, Beijing. The detailed analytical procedures were as described by Cheng et al. (2017). The mass fractionations for Sr and Nd were corrected by $^{86}Sr/^{88}Sr = 0.1194$ and $^{146}Nd/^{144}Nd = 0.7219$, respectively. The $^{87}Sr/^{86}Sr$ value of NIST SRM 987 in this lab was 0.710250 ± 25 (2σ, N = 61) and the $^{143}Nd/^{144}Nd$ value of the Alfa Nd (an ultrapure single elemental standard solution from the Alfa Aesar A Johnson Mattey Company of the USA) was 0.512432 ± 24 (2σ, N = 58). The $^{87}Sr/^{86}Sr$ and $^{143}/^{144}Nd$ ratios of isotopic standard BHVO-2 in our study were measured as 0.703469 ± 11 and 0.512945 ± 9, respectively, coinciding with the published data (Li et al., 2012 and references therein).

Magnesium isotopic analysis was performed at the State Key Laboratory of Geological Processes and Mineral Resources, China University of Geosciences, Beijing, following methods described in previous studies (e.g., Ke et al., 2016; Teng et al., 2007, 2010a; Yang et al., 2009). Fresh clinopyroxene, orthopyroxene and magnetite grains in andesite were handpicked under a binocular microscope. Approximately 500 μg BHVO-2 (Basalt from Havaiian Volcanic Observatory, standard material), 500 μg AGV-2 (Andesite from Guano Valley, standard material), 200 μg BCR-2 (Basalt from Columbia River, standard material), 500–600 μg bulk-rock powders, 150–250 μg clinopyroxene and 150–200 μg orthopyroxene separates were dissolved in Savillex screw-top beakers with a mixture of concentrated HF-HNO_3 (~3:1, v/v) for 48 h at 130 °C until the mixture was completely dissolved. Solutions were evaporated to a dryness at 80 °C and then re-dissolved with a mixture of concentrated HCl-HNO_3 (~3:1, v/v) and a pure concentration of HNO_3 for one or two times in sequence to obtain completely clear solutions. The clear solutions containing ≥60 μg Mg were then dried and dissolved in 1 N HNO_3 ready for an ion exchange column chemistry. Prepared solutions were loaded into the cation exchange columns with pre-cleaned resin (Bio-Rad 200–400 mesh AG50W-×8) two or three times to obtain pure Mg solutions, which were then heated to dryness and dissolved in 3% HNO_3 for mass spectrometry. Magnesium isotopic compositions of the standard materials and our samples were measured on a Neptune Plus MC-ICP-MS in a medium-resolution mode. Each solution was measured at least 4

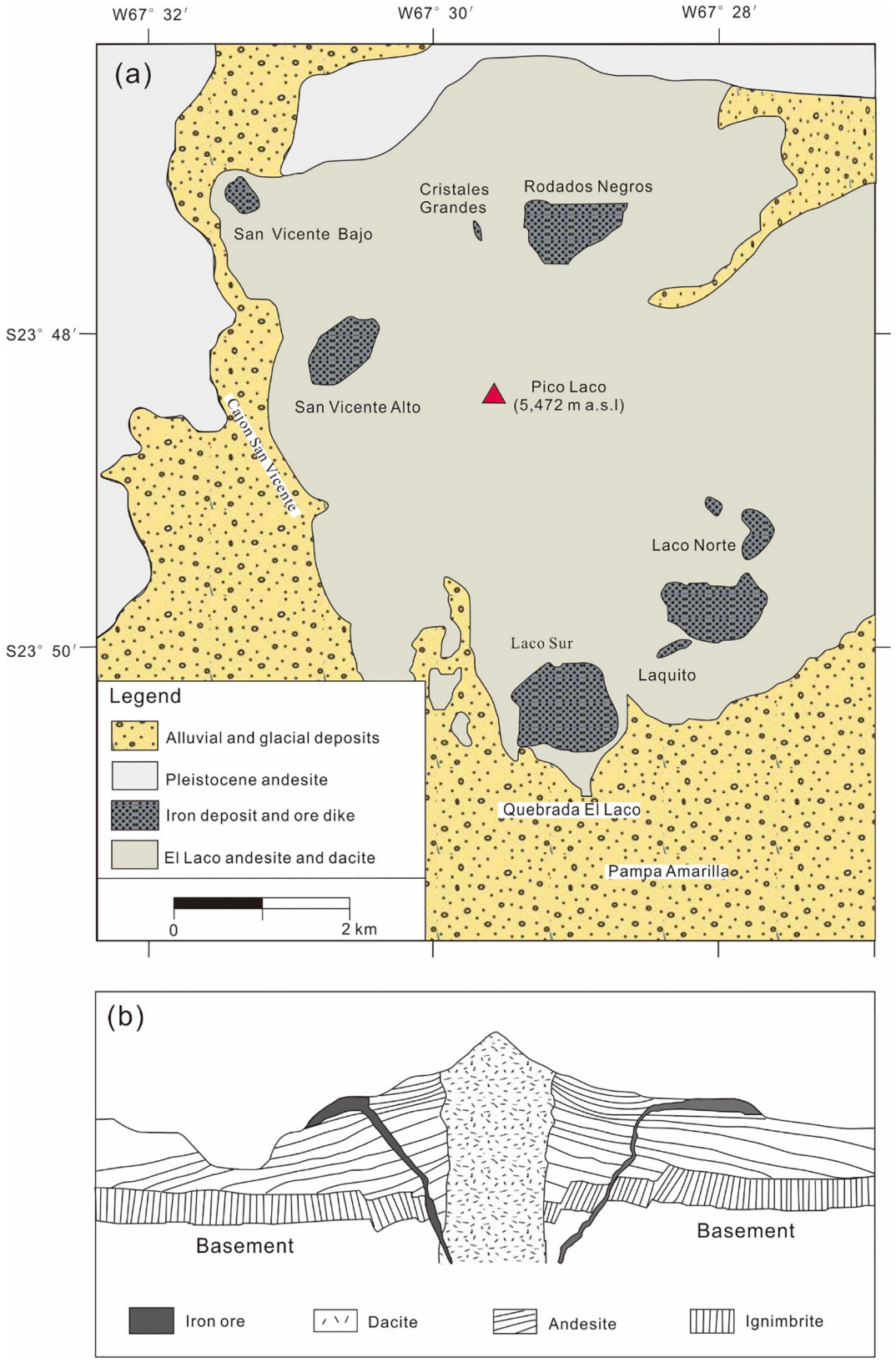

Fig. 2. (a) Geological sketch map of the El Laco volcanic complex, northern Chile (modified from Naranjo et al. (2010)). (b) The profile map of the El Laco volcanic complex and iron deposits, northern Chile.
(Modified after Naslund et al. (2002).)

times to obtain a better reproducibility and accuracy (Ke et al., 2016). The Mg isotopic results were calculated relative to the standard material of the Dead Sea metal Mg standard (DSM3), with the formula $\delta^{26}Mg = [(^{26}Mg/^{24}Mg)_{sample} / (^{26}Mg/^{24}Mg)_{DSM3} - 1] * 1000$. The internal precision in this study is better than ±0.06‰ (2SD) for ^{26}Mg (Ke et al., 2016). Results for these standards including BHVO-2, AGV-2 and BCR-

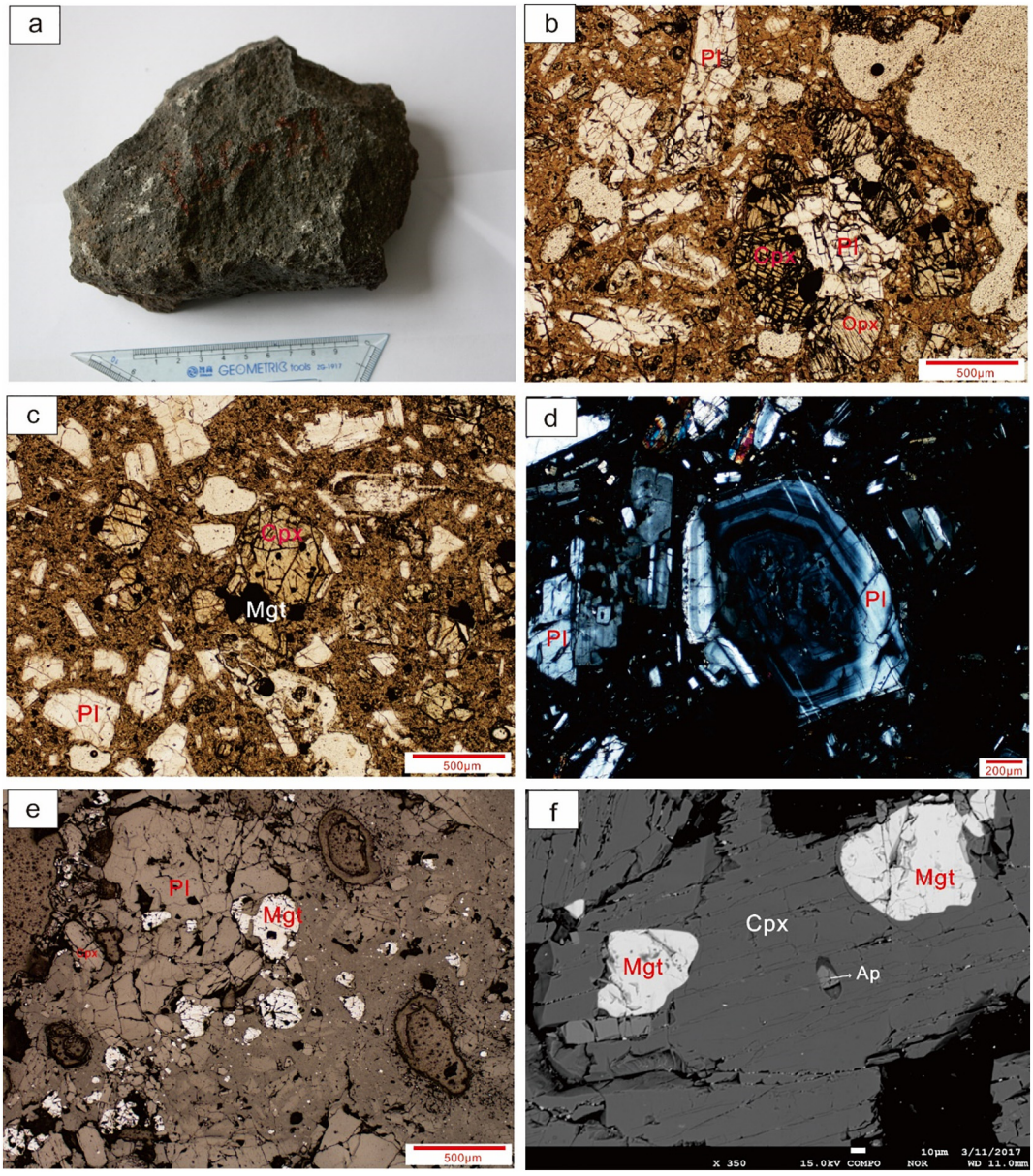

Fig. 3. (a) Hand specimen of fresh andesite, gray to black in color with vesicular structure; (b), (c) optical photomicrographs showing phenocrysts of plagioclase, clinopyroxene and orthopyroxene and porphyritic texture of the andesite (plane-polarized light); (d) optical photomicrographs of zoning plagioclase (cross-polarized light); (f) optical photomicrograph of magnetite in the andesite (reflected-polarized light); (f) BSE image of magnetite and apatite enclosed within the clinopyroxene in the andesite. Abbreviations: pl, plagioclase; cpx, clinopyroxene; opx, orthopyroxene; mgt, magnetite; Ap, apatite.

2 are in agreement with previously published data within errors (Teng, 2017 and references therein). Moreover, the total procedural blank is <10 ng (the average value of the laboratory = 10 ng), making a negligible contribution. The andesitic sample of PLC-21 and the separated orthopyroxene of PLC-13O were excluded, due to some errors during the procedures.

4. Results

4.1. Mineral chemistry

The compositions of representative plagioclase, clinopyroxene, orthopyroxene, magnetite and ilmenite in andesites from the ELVC are presented in Tables A1–4.

The plagioclase is labradorite (An = 50–70) with a compositional range of $Ab_{32.57–45.03}An_{53.53–66.46}Or_{0.77–1.44}$. The clinopyroxene shows a compositional range of $Wo_{33.71–42.07}En_{41.55–43.20}Fs_{14.88–18.95}$ while the compositional range of orthopyroxene is $Wo_{1.44–3.41}En_{66.75–74.95}Fs_{22.19–29.99}$. The temperatures and fO_2 values calculated with the compositions of co-existing magnetite and ilmenite pairs are 876 to 964 °C and −12.32 to −10.36, respectively, very close to the MH (Magnetite-Hematite) oxygen buffer (Fig. 4).

4.2. Bulk-rock major and trace elements

The bulk-rock major and trace element compositions of the andesites are listed in Table 1. The andesites exhibit relatively low MgO contents (2.82–3.56 wt%) and $Mg^{\#}$ values (46–51). They display SiO_2 contents ranging from 55.41 wt% to 60.56 wt%, with restricted TiO_2 (0.86–0.92 wt%), total FeO (FeO^T = 5.82–6.43 wt%), Al_2O_3 (16.08–16.70 wt%) and P_2O_5 (0.19–0.21 wt%) contents. The Na_2O and K_2O contents were 2.72–3.40 wt% and 1.91–2.45 wt%, with K_2O/Na_2O ratios of 0.56–0.85. As shown in Fig. 5, the contents of Al_2O_3, FeO^T, MgO, CaO and P_2O_5 decreased whereas ($Na_2O + K_2O$) increased with

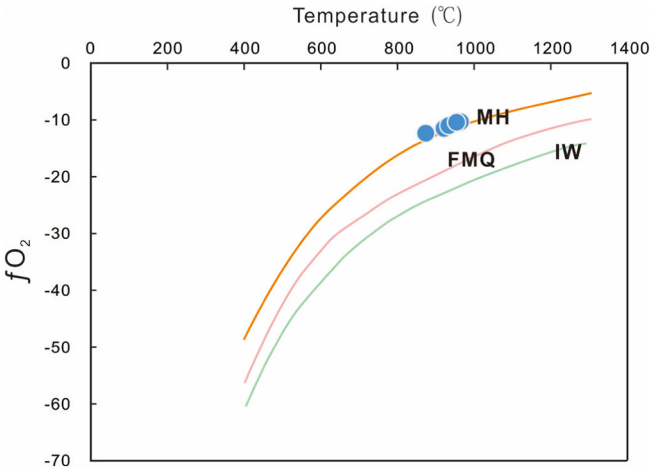

Fig. 4. Calculated magma oxygen fugacity of the El Laco andesite using the major-element data of co-growing magnetite-ilmenite. The MH (Magnetite-Hematite), FMQ (Fayalite-Magnetite-Quartz) and IW (Iron-Wuestite) buffers are from Myers and Eugster (1983).

increasing SiO_2. The K_2O versus SiO_2 diagram shows that the andesites belong to the high-K calc-alkaline series (Fig. 6).

On the primitive-mantle normalized diagram (Fig. 7a), the andesites exhibit characteristics typical of arc magma with a relative enrichment of Rb, U, Th and K and negative Nb, Ta and Ti anomalies. Additionally, the andesites also show depletion of Ba and P, but a slight enrichment of Sr relative to the neighboring elements. On the chondrite-normalized diagram (Fig. 7b), the andesites are characterized by the enrichment of light rare earth elements (LREE) relative to the heavy rare earth element (HREE), with flat HREE patterns. A slight negative Eu anomaly also is displayed by the bulk rocks (Fig. 7b) with $(La/Yb)_N$, $(La/Sm)_N$ and $(Gd/Yb)_N$ in the range of 9.52–10.45, 3.45–3.78 and 1.70–1.98, respectively.

4.3. Sr-Nd-Mg isotopic compositions

Strontium and neodymium isotopic compositions of the andesite are listed in Table 2. The andesites display negative age-corrected $\varepsilon_{Nd}(t)$ ($t = 1.6$ Ma) values ranging from −5.10 to −4.11 and relatively high $(^{87}Sr/^{86}Sr)_i$ ratios of 0.706724–0.707333. Initial $^{143}Nd/^{144}Nd$ values show range of 0.512374 to 0.512425 (Table 2). Additionally, as shown

Table 1
Major (wt%) and trace elements (ppm) compositions of andesites at the El Laco volcanic complex.

Sample	PLC-12	PLC-13	PLC-16	PLC-21	PLC-22	PLC-23	PLC-24	LcSur-3	LcPk-1
SiO_2	56.94	56.99	58.79	58.33	58.39	55.41	59.28	60.56	60.22
TiO_2	0.89	0.89	0.90	0.92	0.88	0.90	0.91	0.88	0.86
Al_2O_3	16.43	16.46	16.44	16.42	16.35	16.08	16.7	16.51	16.32
Fe_2O_3	3.02	3.35	2.94	3.07	2.76	3.63	2.75	3.19	2.64
FeO	3.68	3.42	3.66	3.67	3.62	3.13	3.80	2.95	3.55
MnO	0.10	0.10	0.11	0.11	0.10	0.11	0.11	0.09	0.11
MgO	3.51	3.56	3.22	3.38	3.07	3.55	3.21	3.37	2.82
CaO	6.70	6.67	6.21	6.23	6.43	7.57	6.06	5.36	5.51
Na_2O	2.72	2.75	3.15	3.07	3.13	2.86	3.10	3.40	3.22
K_2O	2.31	2.33	2.22	2.25	2.23	2.05	2.35	1.91	2.45
P_2O_5	0.21	0.21	0.21	0.21	0.21	0.21	0.21	0.19	0.19
LOI	2.83	2.40	1.13	1.00	2.07	3.29	1.03	0.93	1.06
Total	99.34	99.13	98.98	98.66	99.24	98.79	99.51	99.34	98.95
FeO^T	6.40	6.43	6.31	6.43	6.10	6.40	6.27	5.82	5.93
$Mg^{\#}$	49.69	49.90	47.90	48.61	47.52	49.98	47.94	51.03	46.14
Sc	16.0	16.2	16.1	16.6	16.1	16.6	15.9	18	15.1
V	161	165	167	174	161	170	165	168	147
Ga	20.1	20.2	21.0	21.2	20.2	20.1	20.6	21.6	20.4
Rb	72.0	72.1	76.5	75.2	78.4	66.7	76.2	69.7	95.9
Sr	468	466	431	437	429	452	420	419	393
Y	18.8	18.0	19.4	17.8	20.1	19.7	20	20.9	21.3
Zr	156	156	167	162	166	154	165	184	178
Nb	10.5	10.5	11.2	10.8	11.2	10.3	11.2	11.2	11.5
Ba	475	476	491	493	487	451	471	513	508
Hf	4.37	4.46	4.69	4.53	4.65	4.36	4.53	5.37	4.96
Ta	0.75	0.79	0.83	0.76	0.82	0.73	0.81	0.91	0.92
Th	8.57	8.54	9.26	9.29	9.53	7.98	9.12	11.40	10.90
U	1.90	1.80	1.82	1.73	1.87	1.53	1.78	2.17	2.22
Ni	26.9	26.8	22.2	24.0	19.5	28.8	21.5	30.1	17.7
Pb	9.64	8.86	9.92	10.80	10.20	9.06	9.72	13.90	11.00
Co	23.0	22.9	22.5	24.0	21.2	23.9	21.8	20.9	20.1
La	28.4	28.4	29.8	29.3	30.3	28.3	29.8	31.5	32.1
Ce	51.1	50.8	55.0	54.0	55.1	52.3	54.4	58.4	58.5
Pr	7.03	7.03	7.33	7.19	7.39	7.04	7.19	7.78	7.72
Nd	28.3	28.5	29.1	29.0	30.4	28.4	28.9	30.8	30.8
Sm	5.05	5.05	5.32	5.18	5.48	5.29	5.07	5.76	5.47
Eu	1.33	1.31	1.30	1.30	1.27	1.31	1.22	1.35	1.24
Gd	4.41	4.23	4.57	4.38	4.68	4.59	4.48	4.86	4.77
Tb	0.73	0.68	0.74	0.72	0.75	0.74	0.72	0.78	0.76
Dy	3.72	3.58	3.86	3.55	3.92	3.73	3.74	4.24	4.12
Ho	0.69	0.67	0.72	0.66	0.73	0.71	0.70	0.78	0.79
Er	2.04	1.88	2.04	1.87	2.11	2.09	2.03	2.25	2.31
Tm	0.30	0.27	0.31	0.28	0.32	0.30	0.30	0.34	0.35
Yb	1.93	1.84	2.02	1.83	2.17	1.97	1.97	2.26	2.32
Lu	0.30	0.28	0.31	0.27	0.32	0.29	0.29	0.34	0.37

Note: $FeO^T = FeO + 0.8998 * Fe_2O_3$.
$Mg^{\#} = 100 * MgO / (MgO + FeO^T)$, in molar.

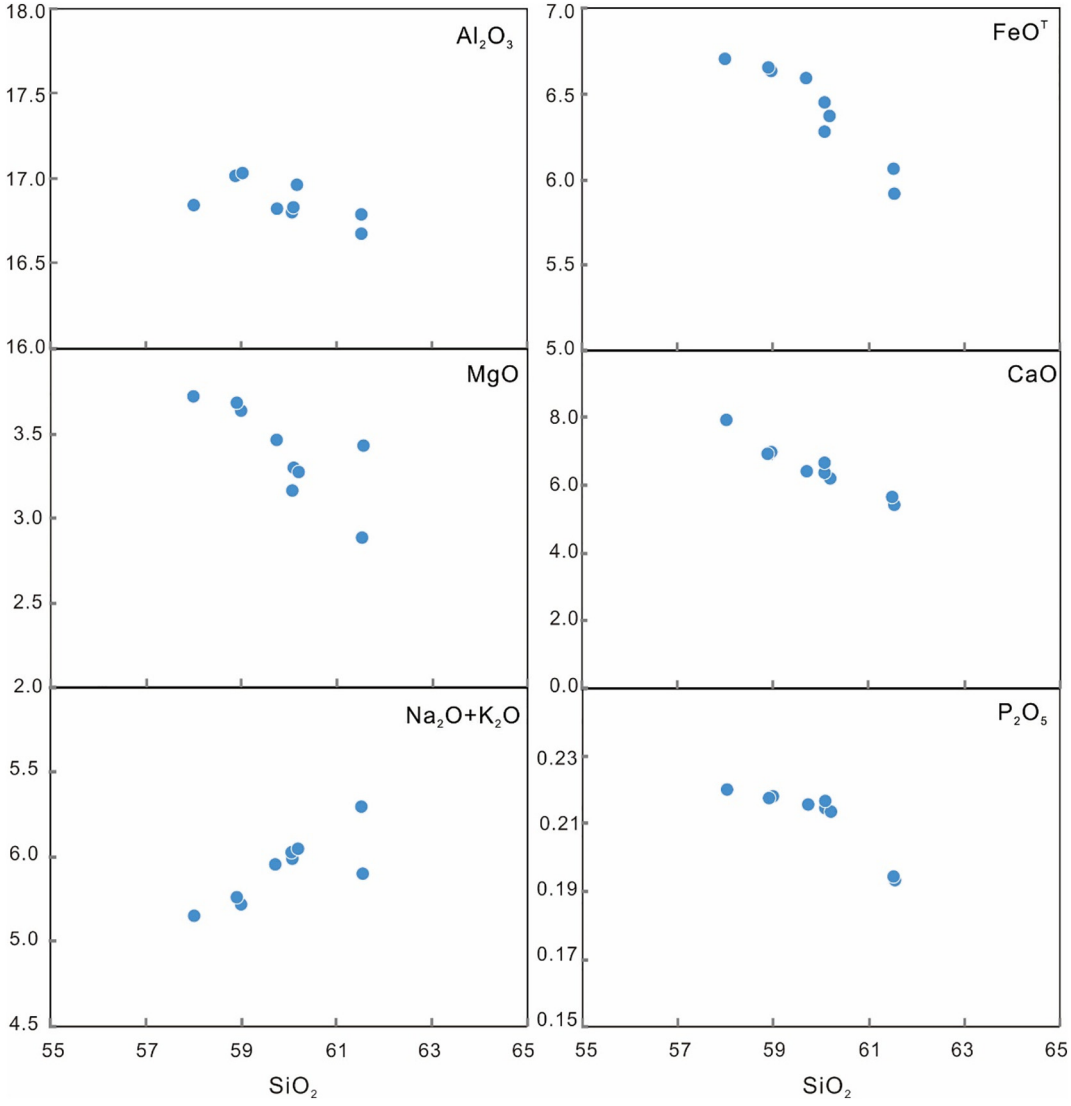

Fig. 5. Harker diagram of the andesites at El Laco.

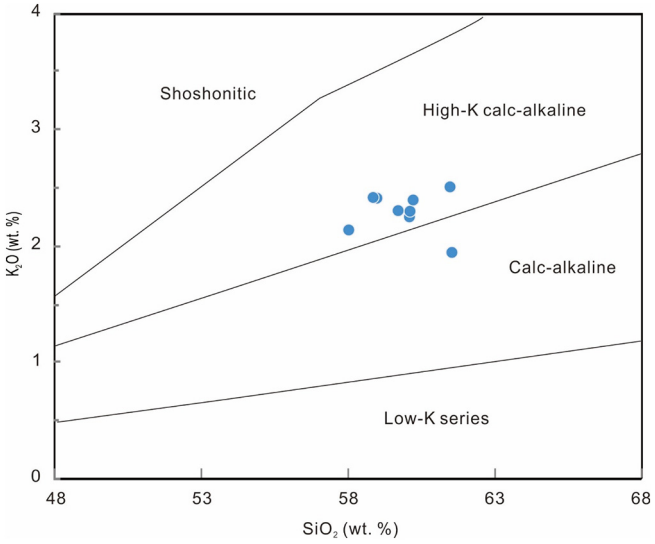

Fig. 6. K_2O vs. SiO_2 plots for the andesites at El Laco. The boundaries are after Wilson (1989).

in Fig. 8, the Sr-Nd isotopic compositions of andesites from the ELVC overlap with those of andesites in the CVZ with ages of <8 Ma.

Magnesium isotopic compositions of the bulk rocks and mineral grains including clinopyroxene, orthopyroxene and magnetite are listed in Table 3. The δ^{26}Mg values of the andesites range from -0.26 ± 0.05‰ to -0.15 ± 0.04‰, with the average value of -0.18 ± 0.05‰, slightly heavier than that of the normal mantle (-0.25 ± 0.07‰; Huang et al., 2011; Lai et al., 2015; Teng et al., 2010a), but similar to that of the oceanic arc lavas (average $\delta^{26}Mg = -0.18$ as reported by Teng et al. (2016), Fig. 9a). The clinopyroxene and orthopyroxene shows δ^{26}Mg values of -0.27 ± 0.03‰ to -0.20 ± 0.04‰ with an average value of -0.24 ± 0.04‰, and -0.24 ± 0.06‰ to -0.18 ± 0.03‰ with an average value of -0.22 ± 0.04‰, respectively, whereas the δ^{26}Mg values of magnetite range from $+0.09 \pm 0.06$‰ to $+0.33 \pm 0.06$‰ with an average value of $+0.23 \pm 0.06$‰. Additionally, a slightly negative correlation between δ^{26}Mg values and SiO_2 contents is also observed in Fig. 9b.

5. Discussion

5.1. Genesis of heavy Mg isotopic compositions

As shown in Table 3 and Fig. 9, the Mg isotopic compositions of the ELVC andesites are slightly heavier than that of the primitive mantle.

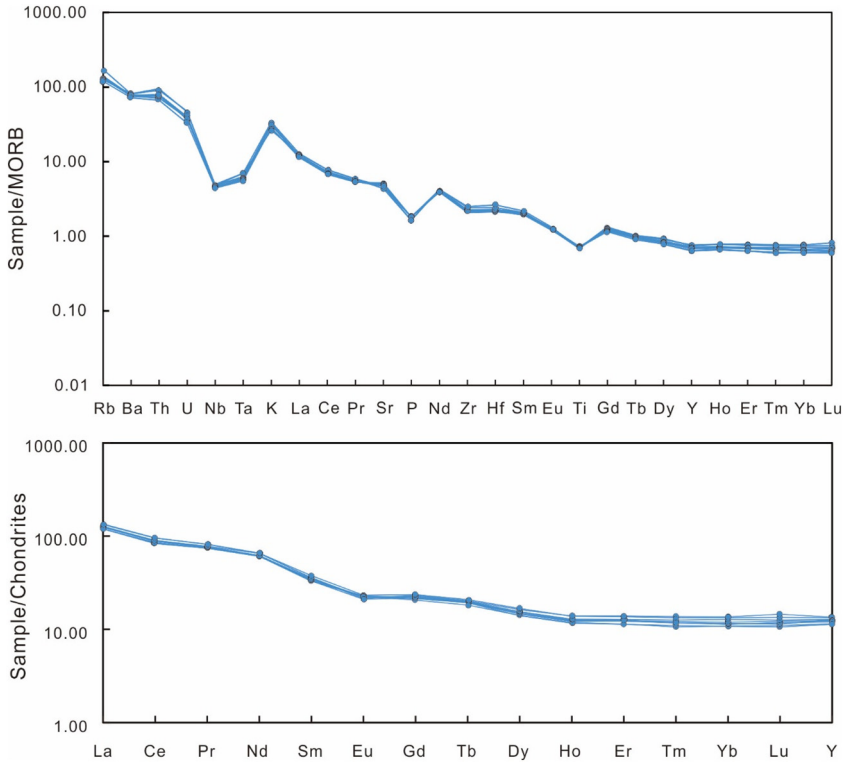

Fig. 7. (a) MORB-normalized spidergram for samples of the El Laco andesites; (b) chondrite-normalized rare element pattern of the El Laco andesite. Normalized values are from Sun and McDonough (1989).

There are several factors that may influence Mg isotopic compositions of continental volcanic rocks, such as surface weathering and alteration, fractional crystallization of the magma, partial melting conditions at a relatively deep level, and the incorporation of crustal materials (continental or oceanic crustal materials) before or during the magmatic evolution.

5.1.1. Effects of chemical weathering and alteration

It is well known that chemical weathering and hydrothermal alteration can mask the actual chemical compositions and $^{87}Sr/^{86}Sr$ ratios of igneous rocks. Furthermore, as reported in previous studies, these processes can also potentially modify the Mg isotopic composition of arc lavas and shift their $\delta^{26}Mg$ to higher values (Ke et al., 2011; Teng et al., 2010b, 2016). However, all samples for geochemical analyses in this study are fresh, as indicated by their low LOI values (0.93–3.29 wt %). Moreover, both the $(^{87}Sr/^{86}Sr)_i$ and $\varepsilon_{Nd}(t)$ of the ELVC andesites display a very small range, indicating that the effect of hydrothermal alteration or weathering was negligible.

5.1.2. Fractional crystallization

The presence of plagioclase, pyroxene, magnetite and apatite in the ELVC andesites indicates that the rocks had experienced fractional crystallization. This inference is also supported by the decreasing trends of Al_2O_3, CaO, MgO, FeO^T and P_2O_5 contents with increasing SiO_2 in Fig. 5. The appearance of magnetite and apatite enclosed in the pyroxene phenocrysts indicates that magnetite and apatite are liquidus minerals, suggesting high oxygen fugacity. This conclusion is also reinforced by the relatively high oxygen fugacity (about MH, i.e., magnetite-hematite oxygen buffer) of the andesitic melt based on the calculation using the magnetite-ilmenite mineral pairs (Table A4, Fig. 4).

Previous studies have demonstrated that the crystallization of minerals does not cause the fractionation of Mg isotope in basaltic and granitic systems (Liu et al., 2010; Teng et al., 2007, 2010a). However, as reported in our paper (Table 3), the pyroxene phenocrysts of ELVC andesites exhibit distinct Mg isotopes from both the whole rock and the magnetite crystals, indicating Mg fractionation during the fractional crystallization of the continental arc andesitic system. Additionally, the continental arc andesites of ELVC contain slightly heavier Mg isotopes

Table 2
Sr-Nd isotopic compositions of andesites at the El Laco volcanic complex.

Sample	Rb(ppm)	Sr(ppm)	$^{87}Rb/^{86}Sr$	$^{87}Sr/^{86}Sr$	(2σ)	Sm(ppm)	Nd(ppm)	$^{147}Sm/^{144}Nd$	$^{143}Nd/^{144}Nd$	(2σ)	$(^{87}Sr/^{86}Sr)_t$	$(^{143}Nd/^{144}Nd)_t$	$\varepsilon_{Nd}(t)$
PLC-12	72.0	468	0.445079	0.706860	9	5.05	28.3	0.107878	0.512423	8	0.706849	0.512422	−4.17
PLC-13	72.1	466	0.447610	0.706853	11	5.05	28.5	0.107121	0.512426	9	0.706842	0.512425	−4.11
PLC-16	76.5	431	0.513510	0.707198	10	5.32	29.1	0.110520	0.512397	9	0.707186	0.512396	−4.69
PLC-21	75.2	437	0.497852	0.707164	12	5.18	29.0	0.107983	0.512388	10	0.707153	0.512387	−4.85
PLC-22	78.4	429	0.528717	0.707192	11	5.48	30.4	0.108976	0.512395	9	0.707180	0.512394	−4.72
PLC-23	66.7	452	0.426906	0.706733	10	5.29	28.4	0.112606	0.512406	8	0.706724	0.512405	−4.50
PLC-24	76.2	420	0.524892	0.707173	10	5.07	28.9	0.106055	0.512385	9	0.707161	0.512384	−4.91
LcSur-3	69.7	419	0.481270	0.707317	11	5.76	30.8	0.113056	0.512375	8	0.707306	0.512374	−5.10
LcPk-1	95.9	393	0.705988	0.707349	8	5.47	30.8	0.107364	0.512390	8	0.707333	0.512389	−4.83

Note: Chondrite uniform reservoir (CHUR) values ($(^{143}Sm/^{144}Nd)_{CHUR} = 0.512638$, $(^{143}Nd/^{144}Nd)_{CHUR} = 0.1967$) are used for the calculation. $Rb = 1.42 \times 10^{-11}$/year (Steiger and Jäger, 1977), $Sm = 6.5 \times 10^{-12}$/year (Lugmair and Harti, 1978). $(^{87}Sr/^{86}Sr)t$ and $\varepsilon_{Nd}(t)$ were calculated at 1.6 Ma.

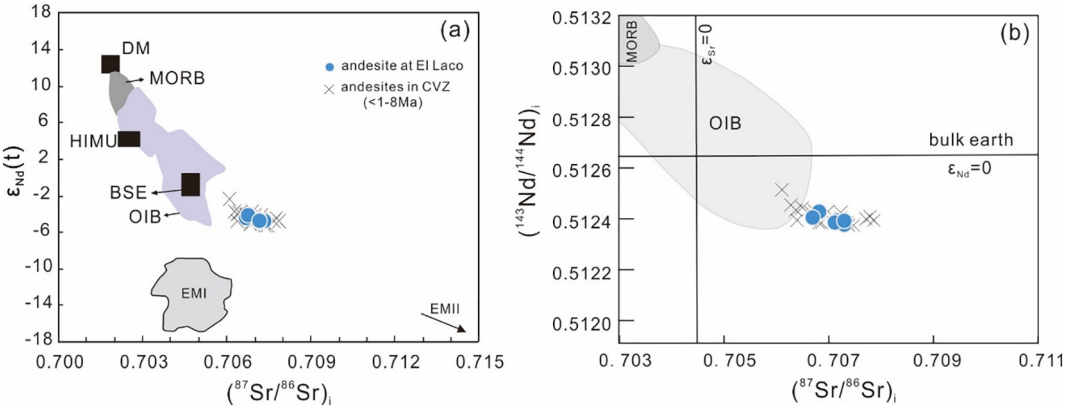

Fig. 8. (a) Initial $^{87}Sr/^{86}Sr$ vs. $\varepsilon_{Nd}(t)$ diagram for the El Laco andesites. Data of DM, HIMU, MORB, OIB, BSE, EMI and EMII were from Hou et al. (2013); (b) initial $^{87}Sr/^{86}Sr$ vs. initial $^{143}Nd/^{144}Nd$ diagram for the El Laco andesites. Data of MORB and OIB were from Wilson (1989). Data of andesites in CVZ with ages <8 Ma were from Richards et al. (2013), Schnurr et al. (2007) and Trumbull et al. (1999).

(average $\delta^{26}Mg = -0.18 \pm 0.05‰$) than that of the primitive mantle ($\delta^{26}Mg = -0.25 \pm 0.07‰$, Teng et al., 2010a).

Previous studies have demonstrated that the equilibrium Mg isotope fractionation was qualitatively controlled by the coordination number of Mg in minerals, with heavy isotopes preferring materials with a low Mg coordination (Liu et al., 2010; Teng, 2017; Urey, 1947). Considering the same coordination number of Mg in plagioclase as in the pyroxene (Mg coordination number = 6), the inter-mineral Mg isotope fractionation between plagioclase and pyroxene is expected to be very limited. Since pyroxene phenocrysts show mantle-like (or slightly heavier) Mg isotopes (Table 3), we infer that the crystallization of these silicate minerals from the melt would not generate the Mg isotopic features of the ELVC andesites which are heavier than that of the primitive mantle. Moreover, many recent studies have revealed that significant Mg isotope fractionation can be induced by oxide (chromite $\delta^{26}Mg = -0.10$ to 0.40‰ and ilmenite $\delta^{26}Mg = -0.50$ to 1.90‰) fractional crystallization and accumulation (e.g., Chen et al., 2018; Su et al., 2017) during the evolution of magma. However, there is no chromite in our samples and that the high oxygen fugacity of the arc andesitic magma (~MH, Fig. 4) does not favor the accumulation of ilmenite. In this case, the main oxide in the andesites is magnetite characterized by significantly heavy Mg isotopes (+0.09 to +0.33‰, Table 3). Thus, crystallization of magnetite would lead to much lighter Mg isotopes of melt residue. Additionally, apatite in the andesites is negligible because of its insignificant amount and low MgO contents. Thus, we conclude that the heavy Mg in ELVC andesites did not originate from the process of fractional crystallization.

Table 3
Magnesium isotopic compositions of andesites at the El Laco volcanic complex and the separated crystals.

Sample	Description	$\delta^{25}Mg$(‰)	2SD	$\delta^{26}Mg$(‰)	2SD
PLC-12	Bulk rock, petrographically fresh	−0.07	0.04	−0.15	0.04
PLC-13	Bulk rock, petrographically fresh	−0.09	0.01	−0.16	0.05
PLC-16	Bulk rock, petrographically fresh	−0.08	0.03	−0.17	0.06
Repeat	Bulk rock, petrographically fresh	−0.09	0.06	−0.18	0.06
PLC-22	Bulk rock, petrographically fresh	−0.08	0.03	−0.18	0.05
PLC-23	Bulk rock, petrographically fresh	−0.08	0.03	−0.16	0.04
PLC-24	Bulk rock, petrographically fresh	−0.08	0.06	−0.18	0.05
LcSur-3	Bulk rock, petrographically fresh	−0.10	0.04	−0.20	0.03
LcPk-1	Bulk rock, petrographically fresh	−0.12	0.02	−0.26	0.05
PLC-12C	Clinopyroxene crystals from PLC-12	−0.11	0.02	−0.22	0.02
PLC-13C	Clinopyroxene crystals from PLC-13	−0.11	0.02	−0.22	0.03
PLC-16C	Clinopyroxene crystals from PLC-16	−0.13	0.04	−0.25	0.05
PLC-21C	Clinopyroxene crystals from PLC-21	−0.13	0.06	−0.25	0.04
PLC-22C	Clinopyroxene crystals from PLC-22	−0.14	0.01	−0.26	0.04
PLC-23C	Clinopyroxene crystals from PLC-23	−0.11	0.05	−0.20	0.04
PLC-24C	Clinopyroxene crystals from PLC-24	−0.12	0.04	−0.24	0.04
LcSur-3C	Clinopyroxene crystals from LcSur-3	−0.12	0.04	−0.25	0.05
LcPk-1C	Clinopyroxene crystals from LcPk-1	−0.14	0.03	−0.27	0.03
PLC-12O	Orthopyroxene crystals from PLC-12	−0.12	0.02	−0.24	0.03
PLC-13O	Orthopyroxene crystals from PLC-13	−0.10	0.03	−0.21	0.03
PLC-21O	Orthopyroxene crystals from PLC-21	−0.08	0.02	−0.18	0.03
PLC-22O	Orthopyroxene crystals from PLC-22	−0.10	0.02	−0.21	0.03
PLC-23O	Orthopyroxene crystals from PLC-23	−0.10	0.05	−0.22	0.05
PLC-24O	Orthopyroxene crystals from PLC-24	−0.10	0.02	−0.20	0.01
LcSur-3O	Orthopyroxene crystals from LcSur-3	−0.12	0.04	−0.24	0.06
LcPk-1O	Orthopyroxene crystals from LcPk-1	−0.11	0.04	−0.22	0.05
PLC-16 M	Magnetite crystals from PLC-16	0.17	0.06	0.33	0.06
PLC-23 M	Magnetite crystals from PLC-23	0.06	0.06	0.09	0.06
PLC-24 M	Magnetite crystals from PLC-24	0.14	0.06	0.25	0.06
AGV-2		−0.09	0.04	−0.16	0.03
BCR-2		−0.11	0.03	−0.22	0.06
BHVO-2		−0.10	0.06	−0.21	0.03
Repeat		−0.11	0.06	−0.23	0.06

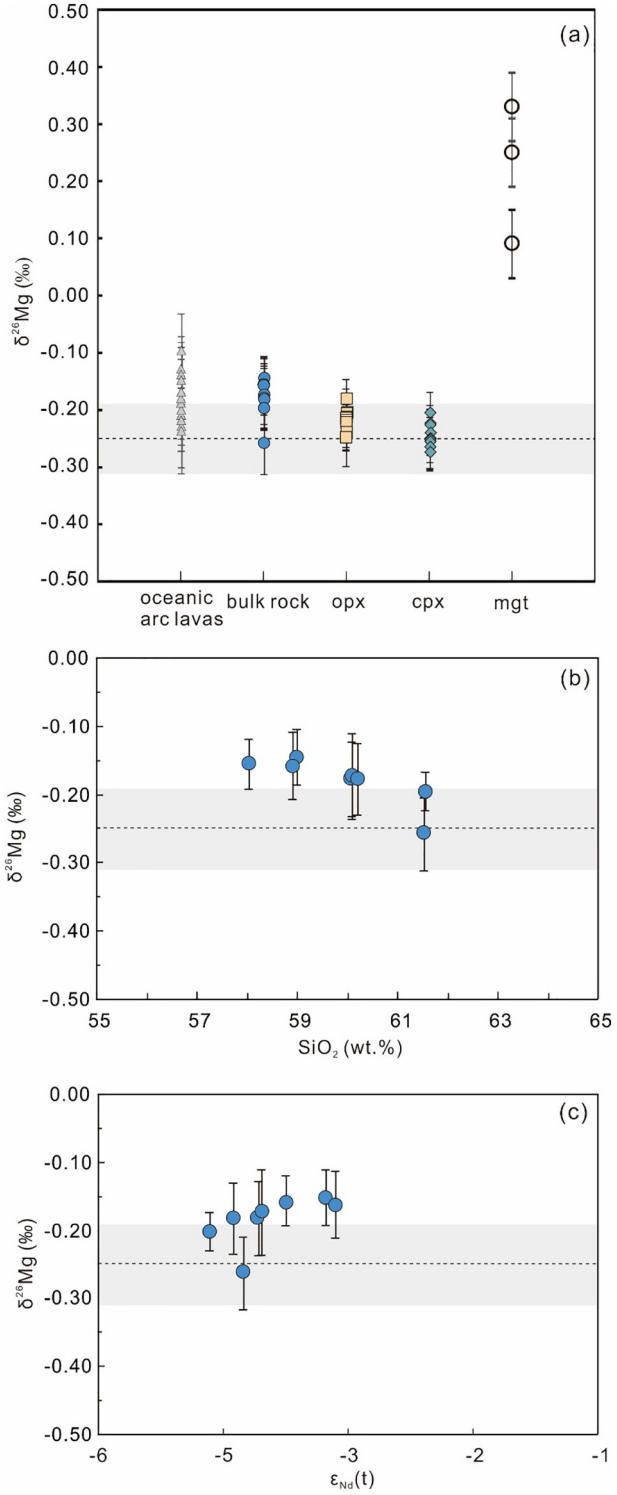

Fig. 9. (a) δ^{26}Mg variation of the El Laco andesites and the separated clinopyroxene, orthopyroxene and magnetite. The δ^{26}Mg of oceanic arc lavas were from Teng et al. (2016); (b) δ^{26}Mg vs. SiO_2 (wt%) for the El Laco andesites; (c) δ^{26}Mg vs. ε_{Nd}(t) diagram for the El Laco andesites. The dashed line represents the average value of the normal mantle. The gray bar presents the composition of the global oceanic basalts (Teng et al., 2010a).

5.1.3. Partial melting of mantle source

Mantle-derived melt is believed to play an important role in the formation of continental arc andesites. Teng et al. (2010a) suggested that the Earth's mantle is homogeneous with an average δ^{26}Mg composition of -0.25 ± 0.07‰ (2SD). Most studies have considered that mantle partial melting does not significantly fractionate Mg isotopes (Teng et al., 2010a, 2016). However, as reported in recent studies (e.g., Stracke et al., 2018; Su et al., 2015; Zhong et al., 2017), the case will be somewhat different when garnet exists in the mantle source, termed the 'garnet effect'. Since garnet has a much larger Mg coordination number of 8, it is always enriched in light Mg isotopes compared to other coexisting silicate minerals (e.g., olivine, pyroxene and plagioclase with Mg coordination number of 6). In this case, arc lavas could potentially be isotopically heavier than the mantle source of peridotite or pyroxenite, with garnet as a residual phase. However, according to the high contents of HREE and the flat HREE patterns displayed by the ELVC andesites (Fig. 7), the possibility of residual garnet in the magma source is excluded, suggesting that the heavier Mg-rich feature of the andesites of ELVC was not caused by the partial melting of the mantle source. Hence, the heavy Mg isotopes of the andesites were most likely attributed to the incorporation of continental and/or oceanic crustal materials in the magma system.

5.2. Implications of petrogenesis on continental arc andesites of ELVC

As discussed above, the heavy Mg isotopes of the andesites suggest the incorporation of crustal materials possibly through source modification or shallow processes such as magma mixing and continental crustal contamination, which is also supported by the enrichment of LILES (e.g., Rb, K, Th and LREEs) and the negative Nb, Ta and Ti anomalies.

5.2.1. Continental crustal contamination and magma mixing

The incorporation of continental crustal materials into the magmatic system is mainly via crustal contamination and magma mixing, processes that would generate similar geochemical and isotopic features. Considering the exceptionally thick continental crust (~60 km) beneath the ELVC (Tassara, 1997), the incorporation of crustal materials during mantle-derived magma ascent is considered to be significant. Since Mg isotopic composition is highly heterogeneous in the continental crust, with δ^{26}Mg of upper continental crust varying from −0.52‰ to +0.92‰ (Li et al., 2010), whereas the δ^{26}Mg of the lower continental crust is in the range of −0.27‰ to +0.19‰ (Teng et al., 2013), either magma mixing or continental crustal contamination during the magma ascent might modify the Mg isotopic composition of igneous lavas.

Both the magma mixing and continental crustal contamination will elevate the abundance of SiO_2, Ba and $^{87}Sr/^{86}Sr$, but lower the ε_{Nd}(t) values. Hence, if the heavy Mg isotopes were mainly derived from the continental crust, a positive correlation between the δ^{26}Mg and SiO_2 contents and a negative correlation between δ^{26}Mg and ε_{Nd}(t) are expected. However, as shown by plots in Fig. 9b, c, the ELVC andesites display the contrasting trends, indicating that neither continental crustal contamination nor magma mixing of continental crust-derived felsic melts (if existent) is the reason for the heavy Mg in andesitic lavas. Additionally, as demonstrated by previous studies, the continental crustal materials incorporated into the El Laco melt were composed predominantly of the Yacoraite Formation (Late Cretaceous), a member of the Late Mesozoic-Tertiary Salta Group located beneath the volcano (e.g., Matthews et al., 1996; Naranjo et al., 2010; Tornos et al., 2017). The Yacoraite Formation is mainly composed of sandstones and carbonate rocks including limestone with high Mg contents and dolomicrite, the later making the formation an excellent marker horizon in the Salta Group (Marquillas et al., 2005). Since the sedimentary carbonate rocks (limestone and dolomite) have been demonstrated to have extremely light δ^{26}Mg values ranging from −5.55‰ to −0.47‰ (e.g., Galy et al., 2002; Higgins and Schrag, 2010; Tipper et al., 2006; Wombacher et al., 2011), the involvement of Yacoraite Formation carbonate rocks would decrease the δ^{26}Mg values of the magma, which is consistent with the negative correlation between the whole-rock δ^{26}Mg and SiO_2 contents, and the positive correlation between the whole-rock δ^{26}Mg and ε_{Nd}(t) values (Fig. 9).

Thus, the heavy Mg isotopic compositions were likely inherited from the subducted materials probably via source modification of sub-arc primitive mantle wedge. Additionally, the El Laco andesites show much lower Ba/Th (45–56), but higher Th/La (0.28–0.38) and Th/Yb (4.05–5.08) ratios than those of the primitive mantle (Ba/Th = 82.22, Th/La = 0.12, Th/Yb = 0.17; e.g., Sun and McDonough, 1989) and the continental crust (Ba/Th = 81.43, Th/La = 0.28, Th/Yb = 2.95; e.g., Rudnick and Gao, 2003), indicating that these elemental ratios might also be attributed to the incorporation of subducted materials.

5.2.2. Contributions of subducted materials to the mantle source

Generally, there are two types of subducted materials incorporated into the mantle source of arc volcanics: 1) aqueous fluids released by the oceanic crust and/or subducted sediments, and 2) hydrous melts derived from the subducted slab (sediments and/or oceanic crust) (Spandler and Pirard, 2013; Zhang et al., 2010; Zheng and Hermann, 2014). It is notable that subducted sediments can be incorporated into the mantle wedge through physical addition under subsolidus conditions (Behn et al., 2011; Marschall and Schumacher, 2012), and/or through chemical reaction of sediment-derived melt with the mantle peridotite at the slab-mantle interface (Zheng, 2012). Considering that the subsolidus sediments in the former case would finally produce extensive melt when they rise into the hot corner of the mantle wedge, and that sediment-derived melts (either in case of physical addition or chemical reaction) will inevitably interact with the surrounding mantle wedge peridotite, we consider incorporation of sediments mainly in the form of melt. However, Mg isotope fractionation was demonstrated to be limited during the metamorphic dehydration of a subducting slab (Li et al., 2011, 2014; Teng et al., 2013; Wang et al., 2014), implying that the dehydrated rocks can preserve the pristine Mg isotopic compositions. As shown by Fig. 7a, the enrichment of LILEs of the ELVC andesites relative to the MORB, suggests the incorporation of subducted fluids into the mantle source. Moreover, barium is a fluid-mobile incompatible trace element and thus susceptible to dissolution in and transport by aqueous fluids, whereas Th is a melt-mobile incompatible trace element and thus susceptible to dissolution and transport by hydrous melts at elevated temperature (Kelemen et al., 2003; Zheng and Hermann, 2014). The ELVC andesites show depletion of Ba (Fig. 7a), as well as much lower Ba/Th but much higher Th/La and Th/Yb ratios than those of the primitive mantle, indicating the involvement of the subducted melts. Therefore, we infer that the mantle source beneath the El Laco was modified by both aqueous fluids and the melts which were derived from the subducted slab.

Additionally, as shown by Fig. 10, δ^{26}Mg of the ELVC andesites become heavy as Ba/Th ratios increase and the Th/La and Th/Yb ratios decrease, demonstrating that the heavy Mg isotopes of the andesites is genetically-linked with the incorporation of hydrothermal fluids derived from the subducted slab by dehydration.

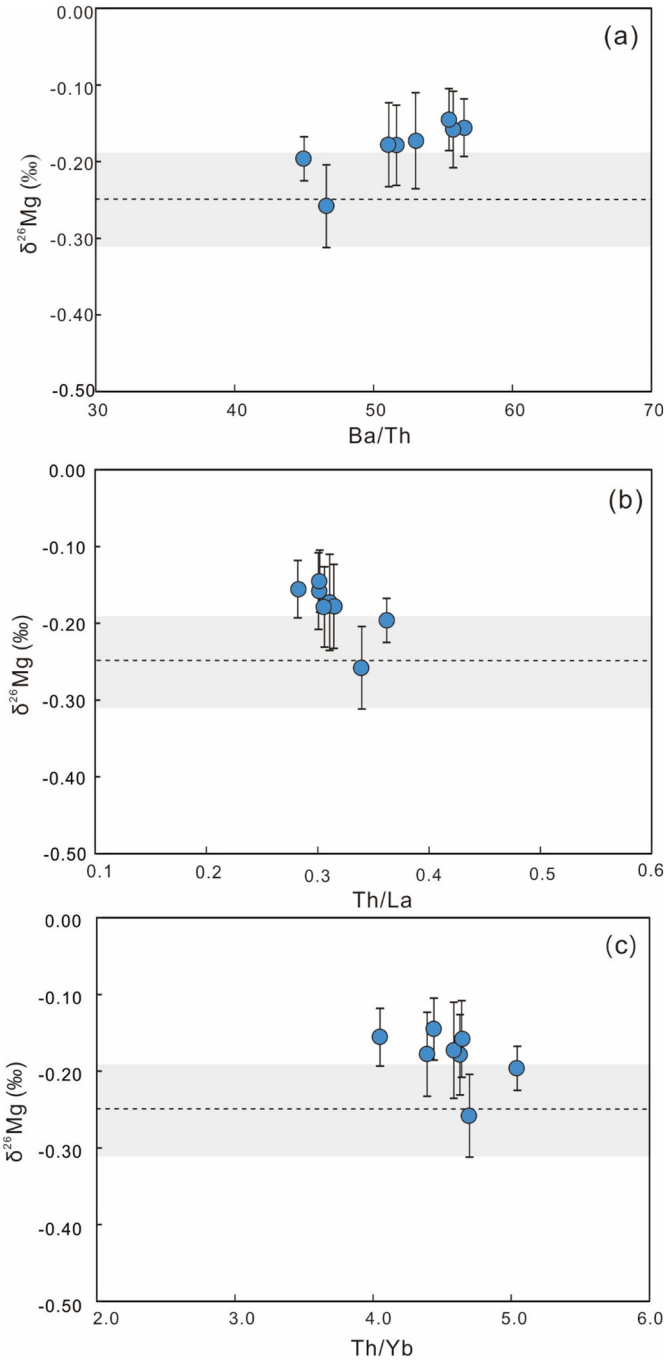

Fig. 10. (a) δ^{26}Mg values vs. Ba/Th ratios diagram for the El Laco andesites; (b) δ^{26}Mg values vs. Th/La ratios diagram for the El Laco andesites; (c) δ^{26}Mg values vs. Th/Yb ratios diagram for the El Laco andesites.

6. Conclusions

This is the first report of the Mg isotopic composition of continental arc lavas from the El Laco volcanic complex in northern Chile. These andesites display slightly heavier Mg isotopic compositions than that of the primitive mantle. Based on our dataset, Mg isotope fractionation was demonstrated to occur during the fractional crystallization process of the arc andesitic system beneath El Lac, and magnetite in the andesites is characterized by a significant enrichment of heavy Mg isotopes. Additionally, our study also shows that both the continental crustal contamination and subducted oceanic slab significantly contributed to the formation of the continental arc lavas. The slightly heavier Mg isotopic compositions of continental arc lavas than that of primitive mantle, are most likely attributed to the incorporation of aqueous fluids derived from the subducted fluids by dehydration, which react with the primitive mantle to produce the metasomatic mantle source of continental arc lavas.

Acknowledgements

We thank Editor Prof. Andrew Kerr and two anonymous referees for their constructive comments and suggestions which helped in improving this paper. Special thanks are given to María Ávila for language editing and Xunan Meng and Ruiying Li for their help in the Mg isotopic analyses. Thanks are also to Compañía Minera del Pacífico, particularly Mario Rojo and Nino Sosa for granting access to the El Laco mining camp. This work was supported by National Nature Science Foundation of China (41472060 and 41390442); and 973 Program (2012CB416806).

Appendix A. Supplementary data

Supplementary data to this article can be found online at https://doi.org/10.1016/j.lithos.2018.08.010.

References

Allmendinger, R.W., Jordan, T.E., Kay, S.M., Isack, B.L., 1997. The evolution of the Altiplano-Puna plateau of the Central Andes. Annu. Rev. Earth Planet. Sci. 25, 139–174.

Armstrong, J.T., 1995. CITZAF – a package of correction programs for the quantitative electron microbean X-ray analysis of thick polished materials, thin films and particles. Microbeam Anal. 4, 117–200.

Behn, M.D., Kelemen, P.B., Hirth, G., Hacker, B.R., Massonne, H.J., 2011. Diapirs as the source of the sediment signature in arc lavas. Nat. Geosci. 4, 641–646.

Chen, L.M., Teng, F.Z., Song, X.Y., Hu, R.Z., Yu, S.Y., Zhu, D., Kang, J., 2018. Magnesium isotopic evidence for chemical disequilibrium among cumulus minerals in layered mafic intrusion. Earth Planet. Sci. Lett. 487, 74–83.

Cheng, Z.G., Zhang, Z.C., Hou, T., Santosh, M., Chen, L.L., Ke, S., Xu, L.J., 2017. Decoupling of Mg-C and Sr-Nd-O isotopes traces the role of recycled carbon in magnesiocarbonatites from the Tarim Large Igneous Province. Geochim. Cosmochim. Acta 202, 159–178.

Frutos, J., Oyarzún, J., 1975. Tectonic and geochemical evidence concerning the genesis of El Laco magnetite lava flow deposits, Chile. Econ. Geol. 70, 988–990.

Frutos, J., Oyarzun, J.M., Shiga, Y., Alfaro, G., 1990. The El Laco magnetite lava flow deposits, northern Chile: an up-to-date review and new data. Soc. Geol. Appl. Miner. Depos. Spec. Publ. 8, 681–690.

Galy, A., Bar-Matthews, M., Halicz, L., O'Nions, R.K., 2002. Mg isotopic composition of carbonate: insight from speleothem formation. Earth Planet. Sci. Lett. 201 (1), 105–115.

Grove, T.L., Parman, S.W., Bowring, S.A., Price, R.C., Baker, M.B., 2002. The role of H_2O rich fluids in the generation of primitive basaltic andesites and andesites from the Mt. Shasta region N. California. Contrib. Mineral. Petrol. 142, 375–396.

Grove, T.L., Till, C.B., Krawczynski, M.J., 2012. The role of H2O in subduction zone magmatism. Annu. Rev. Earth Planet. Sci. 40, 413–439.

Handler, M.R., Baker, J.A., Schiller, M., Bennett, V.C., Yaxley, G.M., 2009. Magnesium stalbe isotope composition of Earth's upper mantle. Earth Planet. Sci. Lett. 282 (1–4), 306–313.

Higgins, J.A., Schrag, D.P., 2010. Constraining magnesium cycling in marine sediments using magnesium isotopes. Geochim. Cosmochim. Acta 74 (17), 5039–5053.

Hildreth, W., Moorbath, S., 1988. Crustal contributions to arc magmatism in the Andes of central Chile. Contrib. Mineral. Petrol. 98, 455–489.

Hou, T., Zhang, Z.C., Santosh, M., Encarnacion, J., Wang, M., 2013. The Cihai diabase in the Beishan region, NW China: Isotope geochronology, geochemistry and implications for Cornwall-style iron mineralization. J. Asian Earth Sci. 70-71, 231–249.

Huang, F., Zhang, Z., Lundstrom, C.C., Zhi, X., 2011. Iron and magnesium isotopic compositions of peridotite xenoliths from Eastern China. Geochim. Cosmochim. Acta 75, 3318–3334.

Ke, S., Liu, S.A., Li, W.Y., Yang, W., Teng, F.Z., 2011. Advances and application in magnesium isotope geochemistry. Acta Petrol. Sin. 27 (2), 383–397 (in Chinese with English abstract).

Ke, S., Teng, F.Z., Li, S.G., Gao, T., Liu, S.A., He, Y.S., Mo, X.X., 2016. Mg, Sr, and O isotope geochemistry of syenites from northwest Xinjiang, China: tracing carbonate recycling during Tethyan oceanic subduction. Chem. Geol. 437, 109–119.

Kelemen, P.B., 1995. Genesis of high Mg# andesites and the continental crust. Contrib. Mineral. Petrol. 120, 1–19.

Kelemen, P.B., Yogodzinski, G.M., School, D.W., 2003. Along-strike variation in the Aleutian island arc: genesis of high Mg# andesite and implications for continental crust. Geophys. Monogr. Ser. 138, 223–276.

Lai, Y.J., Pogge von Strandmann, P., Dohmen, R., Takazawa, E., Elliott, T., 2015. The influence of melt infiltration on the Li and Mg isotopic composition of the Horoman Peridotite Massif. Geochim. Cosmochim. Acta 164, 318–332.

Lee, C.T.A., Morton, D.M., Kistler, R.W., Baird, A.K., 2007. Petrology and tectonics of Phanerozoic continent formation: from island arcs to accretion and continental arc magmatism. Earth Planet. Sci. Lett. 263, 370–387.

Li, W.Y., Teng, F.Z., Ke, S., Rudnick, R.L., Gao, S., Wu, F.Y., Chappell, B., 2010. Heterogeneous magnesium isotopic composition of the upper continental crust. Geochim. Cosmochim. Acta 74, 6867–6884.

Li, W.Y., Teng, F.Z., Xiao, Y., Huang, J., 2011. High-temperature inter-mineral magnesium isotope fractionation in eclogite from the Dabie orogen, China. Earth Planet. Sci. Lett. 304, 224–230.

Li, C.F., Li, X.H., Li, Q.L., Guo, J.H., Li, J.H., Li, X.H., Yang, Y.H., 2012. Rapid and precise determination of Sr and Nd isotopic ratios in geological samples from the same filament loading by thermal ionization mass spectrometry employing a single-step separation scheme. Anal. Chim. Acta 727, 54–60.

Li, W.Y., Teng, F.Z., Wing, B.A., Xiao, Y., 2014. Limited magnesium isotope fractionation during metamorphic dehydration in metapelites from the Onawa contact aureole, Maine. Geochem. Geophys. Geosyst. 15, 408–415.

Liu, S.A., Teng, F.Z., He, Y.S., Ke, S., Li, S.G., 2010. Investigation of magnesium isotope fractionation during granite differentiation: Implication for Mg isotopic composition of the continental crust. Earth Planet. Sci. Lett. 297, 646–654.

Lugmair, G.M, Harti, K., 1978. Lunar initial $^{143}Nd/^{144}Nd$: differential evolution of the lunar crust and mantle. Earth Planet. Sci. Lett. 39, 349–357.

Marquillas, R.A., Papa, C., Sabino, I.F., 2005. Sedimentary aspects and paleoenvironmental evolution of a rift basin: Salta Group (Cretaceous-Paleogene), northwestern Argentina. Int. J. Earth Sci. 94, 94–113.

Marschall, H.R., Schumacher, J.C., 2012. Arc magmas sourced from mélange diapirs in subduction zones. Nat. Geosci. 5, 862–867.

Matthews, S.J., Marquillas, R.A., Kemp, A.J., Grange, F.K., Gardeweg, M.C., 1996. Active skarn formation beneath Láscar volcano, northern Chile: a petrographic and geochemical study of xenoliths in eruption products. J. Metamorph. Geol. 14, 509–530.

Myers, J., Eugster, H.P., 1983. The system Fe-Si-O: oxygen buffer calibrations to 1500 K. Contrib. Mineral. Petrol. 82, 75–90.

Naranjo, J., Henríquez, F., Nyström, J., 2010. Subvolcanic contact metasomatism at El Laco volcanic complex, Central Andes. Andean Geol. 37 (1), 110–120.

Naslund, H.R., Henríquez, F., Nyström, J.O., Vivallo, W., Dobbs, F.M., 2002. Magmatic iron ores and associated mineralization: examples from the Chilean High Andes and Coastal Cordillera. In: Porter, T.M. (Ed.), Hydrothermal Iron Oxide Copper-Gold & Related Deposits: A Global Perspective. 2. Porter GeoConsultancy (PGC) Publishing, Adelaide, pp. 207–226.

Norrish, K., Chappell, B.W., 1977. X-ray fluorescence spectrometry. In: Zussman, J. (Ed.), Physical Methods in Determinative Mineralogy, Second ed. Academic Press, New York, pp. 201–272.

Qi, L., Hu, J., Gregoire, D.C., 2000. Determination of trace elements in granites by inductively coupled plasma mass spectrometry. Talanta 51, 507–513.

Reubi, O., Blundy, J., 2009. A dearth of intermediate melts at subduction zone volcanoes and the petrogenesis of arc andesites. Nature 461 (29), 1269–1274.

Richards, J.P., Jourdan, F., Creaser, R.A., Maldonado, G., DuFrane, S.A., 2013. Geology, geochemistry, geochronology, and economic potential of Neogene volcanic rocks in the Laguna Pedernal and Saldar de Aguas Calientes segments of the Archibarca lineament, northwest Argentina. J. Volcanol. Geotherm. Res. 258, 47–73.

Rudnick, R.L., 1995. Making continental crust. Nature 378, 571–578.

Rudnick, R., Gao, S., 2003. The role of lower crust recycling in continent formation. Geochim. Cosmochim. Acta 67, 1–10.

Schnurr, W.B.W., Trumbull, R.B., Clavero, J., Hahne, K., Siebel, W., Gardeweg, M., 2007. Twenty-five million years of silicic volcanism in the southern central volcanic zone of the Andes: Geochemistry and magma genesis of ignimbrites from 25 to 27 °S, 67 to 72 °W. J. Volcanol. Geotherm. Res. 166, 17–46.

Spandler, C., Pirard, C., 2013. Element recycling from subducting slabs to arc crust: a review. Lithos 170-171, 208–223.

Steiger, R.H., Jäger, E., 1977. Subcommission on geochronology: convention on the use of decay constants in geochronology and cosmochronology. Earth Planet. Sci. Lett. 36, 359–362.

Stracke, A., Tipper, E.T., Klemme, S., Bizimis, M., 2018. Mg isotope systematics during magmatic processes: inter-mineral fractionation in mafic to ultramafic Hawaiian xenoliths. Geochim. Cosmochim. Acta 226, 192–205.

Su, B.X., Teng, F.Z., Hu, Y., Shi, R.D., Zhou, M.F., Zhu, B., Liu, F., Gong, X.H., Huang, Q.S., Xiao, Y., Chen, C., He, Y.S., 2015. Iron and magnesium isotope fractionation in oceanic lithosphere and sub-arc mantle: perspectives from ophiolites. Earth Planet. Sci. Lett. 430, 523–532.

Su, B.X., Hu, Y., Teng, F.Z., Qin, K.Z., Bai, Y., Sakyi, P.A., Tang, D.M., 2017. Chromite-induced magnesium isotope fractionation during mafic magma differentiation. Sci. Bull. 62, 1538–1546.

Sun, X.S., McDonough, W.F., 1989. Chemical and isotopic systematic basalt, implication for mantle composition and processes. Geol. Soc. Lond. Spec. Publ. 42, 313–345.

Tassara, A., 1997. Segmentación andina desde el análisis flexural de la anomalía de Bouger. (M. Sc. Thesis). 140. Universidad de Chile, Santiago.

Tatsumi, Y., 2006. High-Mg andesites in the Setouchi volcanic belt, southwestern Japan: analogy to Archean magmatism and continental crust formation? Annu. Rev. Earth Planet. Sci. 34, 467–499.

Taylor, S.R., 1967. The origin and growth of continents. Tectonophysics 4, 17–34.

Teng, F.Z., 2017. Magnesium isotope geochemistry. Rev. Mineral. Geochem. 82, 219–287.

Teng, F.Z., Wadhwa, M., Helz, R.T., 2007. Investigation of magnesium isotope fractionation during basalt differentiation: implications for a chondritic composition of the terrestrial mantle. Earth Planet. Sci. Lett. 261, 84–92.

Teng, F.Z., Li, W.Y., Ke, S., Marty, B., Dauphas, N., Huang, S., Wu, F.Y., Pourmand, A., 2010a. Magnesium isotope composition of the Earth and chondrites. Geochim. Cosmochim. Acta 74, 4150–4166.

Teng, F.Z., Li, W.Y., Rudnick, R.L., Gardner, L.R., 2010b. Contrasting lithium and magnesium isotopic fractionation during continental weathering. Earth Planet. Sci. Lett. 300, 63–71.

Teng, F.Z., Yang, W., Rudnick, R.L., Hu, Y., 2013. Heterogeneous magnesium isotopic composition of the lower continental crust: a xenolith perspective. Geochem. Geophys. Geosyst. 14, 3844–3856.

Teng, F.Z., Yan, H., Chauvel, C., 2016. Magnesium isotope geochemistry in arc volcanism. Proc. Natl. Acad. Sci. 113, 7082–7087.

Tipper, E.T., Galy, A., Gaillardet, J., Bickle, M.J., Elderfield, H., Carder, E.A., 2006. The magnesium isotope budget of the modern ocean: constraints from riverine magnesium isotope ratios. Earth Planet. Sci. Lett. 250 (1–2), 241–253.

Tornos, F., Velasco, F., Hanchar, J.M., 2016. Iron-rich melts, magmatic magnetite, and superheated hydrothermal systems: the El Laco deposit, Chile. Geology 44 (6), 427–430.

Tornos, F., Velasco, F., Hanchar, J.M., 2017. The magmatic to magmatic-hydrothermal evolution of the El Laco deposit (Chile) and its implications for the genesis of magnetite-apatite deposits. Econ. Geol. 112, 1595–1628.

Trumbull, R.B., Wittenbrink, R., Hahne, K., Emmermann, R., Büsch, W., Gerstenberger, H., Siebel, W., 1999. Evidence for Late Miocene to Recent contamination of arc andesites by crustal melts in the Chilean Andes (25–26°S) and its geodynamic implications. J. S. Am. Earth Sci. 12, 135–155.

Urey, H.C., 1947. The thermodynamic properties of isotopic substances. J. Chem. Soc. (Lond.) 562–581.

Velasco, F., Tornos, F., Hanchar, J.M., 2016. Immiscible iron- and silica-rich melts and magnetite geochemistry at the El Laco volcano (northern Chile): evidence for a magmatic origin for the magnetite deposits. Ore Geol. Rev. 79, 346–366.
Wang, S.J., Teng, F.Z., Li, S.G., Hong, J.A., 2014. Magnesium isotopic systematics of mafic rocks during continental subduction. Geochim. Cosmochim. Acta 143, 34–48.
Wei, R., Gao, Y., Xu, S., Xin, H., Santosh, M., Liu, Y., Lei, S., 2017. The volcanic succession of Baoligaomiao, central Inner Mongolia: evidence for Carboniferous continental arc in the central Asian orogenic belt. Gondwana Res. 51, 234–254.
Wilson, M., 1989. Igneous Petrogenesis. Springer, pp. p191–p225.
Wombacher, F., Eisenhauer, A., Bohm, F., Guessone, N., Regenberg, M., Dullo, W.C., Rüggeberg, A., 2011. Magnesium stable isotope fractionation in marine biogenic calcite and aragonite. Geochim. Cosmochim. Acta 75 (19), 5797–5818.
Yang, W., Teng, F.Z., Zhang, H.F., 2009. Chondritic magnesium isotopic composition of the terrestrial mantle: a case study of peridotite xenoliths from the North China craton. Earth Planet. Sci. Lett. 288 (3–4), 475–482.
Zandt, G., Velasco, A.A., Beck, S.L., 1994. Composition and thickness of the southern Altiplano crust, Volivia. Geology 22, 1003–1006.
Zhang, D.Y., Zhang, Z.C., Xue, C.J., Zhao, Z.D., Liu, J.L., 2010. Geochronology and Geochemistry of the ore-forming porphyries in the Lailisigao'er-Lamasu region of the Western Tianshan Mountains, Xinjiang, NW China: implications for petrogenesis, metallogenesis, and tectonic setting. J. Geol. 118, 543–563.
Zheng, Y.F., 2012. Metamorphic chemical geodynamics in continental subduction zones. Chem. Geol. 328, 5–48.
Zheng, Y.F., Hermann, J., 2014. Geochemistry of continental subduction-zone fluids. Earth Planets Space 66, 93.
Zhong, Y., Chen, L.H., Wang, X.J., Zhang, G.L., Xie, L.W., Zeng, G., 2017. Magnesium isotopic variation of oceanic island basalts generated by partial melting and crustal recycling. Earth Planet. Sci. Lett. 463, 127–135.
Zhu, M.S., Miao, L.C., Yang, S.H., 2013. Genesis and evolution of subduction-zone andesites: evidence from melt inclusions. Int. Geol. Rev. 55 (10), 1179–1190.